IEEE Access
Multidisciplinary ⋮ Rapid Review ⋮ Open Access Journal

Received 28 March 2024, accepted 11 April 2024, date of publication 15 April 2024, date of current version 26 April 2024.

Digital Object Identifier 10.1109/ACCESS.2024.3389501

RESEARCH ARTICLE

5G mm-Wave Technology: Innovative Design of Integrating mm-Wave Wideband Antenna With a Compact CP Microwave Antenna for Diverse Applications

ELAGANDULA APARNA, (Graduate Student Member, IEEE), GOPI RAM, (Senior Member, IEEE), AND G. ARUN KUMAR, (Senior Member, IEEE)
National Institute of Technology at Warangal, Warangal 506004, India
Corresponding author: Gopi Ram (gopi.ram@nitw.ac.in)

ABSTRACT A compact dual-band antenna with a large frequency ratio and wideband mm-wave capabilities, incorporating multiple input multiple outputs (MIMO) technology, and designed for high isolation proposed for 5G applications. It contains a substrate-integrated waveguide (SIW) fractal Koch surface (FKS) slot antenna and a patch with L-shaped slots. A wideband performance is achieved by incorporating a novel FKS slot in SIW during ka-band operation. An L-shaped slot on a coaxial-fed microstrip patch is analysed to achieve circular polarisation in a sub-7 GHz band. The suggested wideband antenna attains improved diversity performance within MIMO systems. A prototype of the proposed antenna is fabricated. Measured results coincide aptly with simulated data. The low-frequency antenna operates at 4.8 and 6.29 GHz with a gain of 4.35 and 3.8 dBi and radiation efficiency of 85 and 88%, respectively. The mm-wave antenna operates from 27.1 to 33.2 GHz, with a bandwidth of 20.3% with a gain of 8.5 dBi and a peak efficiency of 93%. Isolation of $\geq$ 50 and $\geq$ 20 dB is achieved at low and high frequencies, respectively. Envelope correlation coefficient (ECC) value $\leq$ 0.001 and channel capacity loss (CCL) 0.1 bits/sec/Hz. The proposed MIMO systems exhibit lower Bit Error Rate (BER) performance over the AWGN channel. The design shows significant potential for application in mm-wave massive MIMO base station applications.

INDEX TERMS 5G, aperture sharing, circular polarization, FKS slot, FR1 band, FR2 band, large frequency ratio, MIMO, SIW.

I. INTRODUCTION

These days, 5G and beyond technology has attractive features like high data rates compared to 4*G*, ultra-low latency, massive connectivity, diverse frequency bands, and beamforming technology [1]. These features are enhanced by operating at Ka-bands, and despite that, this high-frequency operation faces difficulties with high propagation and atmospheric losses [2], [3], [4]. To avoid these losses, the current 5G spectrum allocated to the sub-7 GHz band (FR1: 410 MHz-7.125 GHz) and mm-wave band (FR2: 24.25-52.6 GHz) [5], [6]. Operating in dual-band, 5G systems can extend coverage to wider areas in the sub-7 GHz band while achieving higher data rates in the Ka-band. This dual-band operation with a large frequency ratio applies to significant use cases, including fixed wireless access, intelligent cities, vehicular communication, and industrial applications [7]. In [8] the incorporation of mm-wave and non-mm-wave antennas into mobile phones for diverse practical perspectives is discussed. For this reason, several 5G communication systems are built with sub-7 GHz band and Ka-band to fulfil the application [9]. A dual-polarized Ka-band antenna array designed for end-fire radiation integrated into mobile devices was subjected to performance evaluation, incorporating a sub-6 GHz band antenna within mobile devices [10]. While [11] explores the performance of a

The associate editor coordinating the review of this manuscript and approving it for publication was Hussein Attia.

Ka-band MIMO terminal dual-polarized quasi-Yagi-Uda antenna. In [12], the concept of the slot's dual functionality is presented. Specifically, a short-circuit varactor diode slot is selected for operation in 4G and WLAN applications. Meanwhile, the same slot, connected with parallel feeders, functions as part of a connected slotted antenna array, offering a wideband operation from 23 to 29 GHz. In [13], a hepta-band antenna design is introduced, incorporating both SIW-slotted antennas and a T-shaped probe. The outer surface of the meandered SIW functions as a strip line, operating at frequencies significantly below its cutoff. This arrangement is combined with the T-shaped probe to enable operation within the sub-6 GHz band. Additionally, SIW-slotted structures cover the 28 and 38 GHz frequency bands. In [14], a thick patch antenna operating in dual bands (S/Ka) is exhibited, featuring 16 slotted cavity elements and showing linear polarization (LP) at both frequency bands. In [15], a WI-FI monopole antenna and a WiGig patch antenna are designed and separated by a compact microstrip resonant cell (CMRC) structure to provide isolation between both antennas. However, this design operates at dual-band with low efficiency. In [16], a tapered slot array structure is designed as a feed structure to a sub-6 GHz dipole antenna and behaves as an array of radiators at the Ka-band. In [14], [15], [16], [17], those proposed dual-band antennas are limited to LP only. Instead of designing LP antennas, circularly polarized (CP) antennas reduce the multipath effects and polarization mismatches in communication [18]. In [19], a dual-band CP SIW slot antenna and patch antenna operating at X and C bands are presented, but this does not meet the criteria of 5G operating bands. In [20], an aperture-coupled circular patch antenna with circular polarization is integrated with a linear polarized SIW slot antenna for dual-band operation. However, this structure is implemented in a multilayer model, which increases fabrication costs. This study presents a single-layer integrated dual-polarized sub-7 GHz/Ka-band antenna design, highlighting key advantages:

1. Implementing an antenna with a significantly large frequency ratio between the Ka-band and sub-6 GHz band elements facilitates their coexistence within a compact area.
2. Developing a dual-polarized antenna incorporating a patch antenna for circular polarization (CP) in the sub-7 GHz band and an SIW slot antenna for linear polarization (LP) in the Ka-band.
3. Achieving broad bandwidth performance through integrating a fractal Koch surface (FKS) slot array into the SIW structure.
4. Designing a Multiple Input Multiple Output (MIMO) SIW FKS slot antenna and evaluating essential parameters like envelope correlation coefficient (ECC), diversity gain (DG), channel capacity loss (CCL), and MIMO antenna bit error rate (BER) performance.

The study is structured as follows: Section II outlines the design methodology for both the sub-7 GHz antenna and the Ka-band antenna. Section III presents results and discussions, followed by Section IV, which focuses on MIMO system performance in communication. Finally, Section V concludes the study.

II. DESIGN METHODOLOGY

For the design of the proposed structure, an RT5880 substrate with a thickness of 0.508*mm* and dielectric properties ($\varepsilon_r = 2.2$, $tan\delta = 0.001$) is selected in the Computer Simulation Tool Microwave Studio (CST MWS) EM tool. The structure configuration covers an area of $26 \times 26\ mm^2$ and incorporates sub-7 GHz band and Ka-band antennas. To fulfil MIMO (Multiple Input Multiple Output) terminal applications, four SIW slot antenna structures are positioned at the four corners of the substrate, as illustrated in Fig. 1. The remaining portion of the substrate is then utilised to design a sub-7 GHz band antenna. The process of modifying the patch shape with inverted L-shape slots is depicted in Fig. 1(b) and (c). Utilising the working principle of SIW, which rejects low-frequency signal transmission, a substantial isolation level is attained by integrating the low-frequency antenna and Ka-band antennas, as illustrated in Fig. 1(d). The design procedures for the Ka-band antenna and sub-7 GHz band antenna are detailed in the subsequent sub-sections.

A. A CIRCULARLY POLARIZED ANTENNA DESIGN FOR SUB-7 GHZ BAND

As depicted in Fig. 1(d), the upper layer of the patch antenna incorporates four L-shaped slots positioned at the ends of the patch edges. The bottom layer shows the coaxial feed point. A TM_{010} mode propagates through the patch and resonates at X-band. For designing a sub-7 GHz band antenna, the patch undergoes modification by etching inverted L-shaped slots along the four edges, as illustrated in Steps II, III, and IV of Fig. 1. As depicted in Fig.2, it is evident that the initial design (Step-I) of the antenna functions at a frequency of 9 GHz (X-band). The dimensions, including width (Wp) and length (Lp), are computed using the following Eq. 1 and Eq. 2 [21]. Where ε_{eff}, ΔL are calculated using the Eq. 3, and Eq. 4 [21].

$$L = \frac{c}{2f_r\sqrt{\varepsilon_{eff}}} - 2\Delta L \tag{1}$$

$$W = \frac{c}{2f_r}\sqrt{\frac{2}{\varepsilon_r + 1}} \tag{2}$$

$$\varepsilon_{eff} = \frac{\varepsilon_r + 1}{2} + \frac{\varepsilon_r - 1}{2}\left[1 + 12\frac{h}{w}\right]^{-1/2} \tag{3}$$

$$\Delta L = 0.412 * h\frac{\left(\varepsilon_{eff} + 0.3\right)\left(\frac{W}{h} + 0.264\right)}{\left(\varepsilon_{eff} - 0.258\right)\left(\frac{W}{h} + 0.8\right)} \tag{4}$$

Designing a patch antenna with a low resonant frequency within a defined area is challenging. The resonating frequency of the patch antenna can be reduced through a series of steps involving the introduction of inverted L-shaped

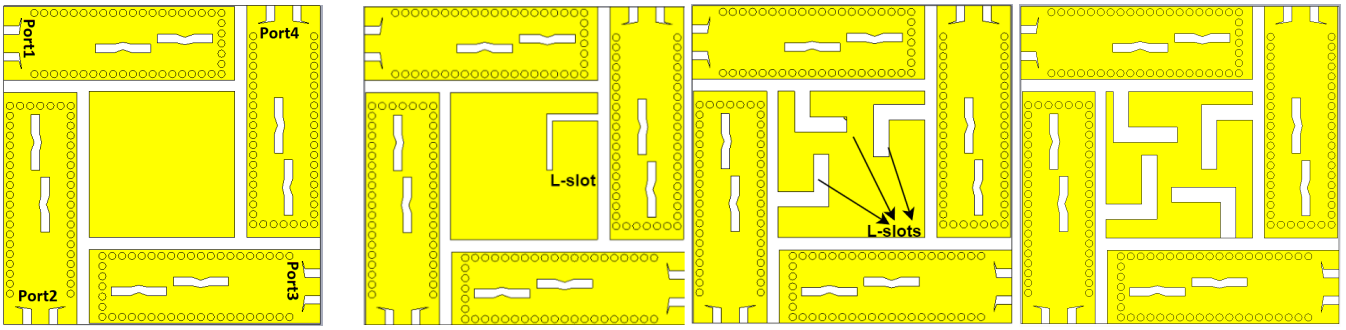

FIGURE 1. The design steps for a compact sub-7 GHz band antenna to operate at sub-7 GHz are outlined as follows: (a) Step-I: the microstrip patch operating at 9 GHz, (b) Step-II: An inverted L-shape slots embedded in patch, (c) Step-III: three inverted L-shape slots covering the edge of patch, and (d) Step-IV: four L-shape slots cutting the edges of patch.

slots. In Step II, a single L-shaped slot with long length (l1) and short length (l2) is etched across the edge of the patch to modify its radiating length, resulting in an operational frequency of 9 GHz. In Step III, two slots are placed oppositely along the radiating edges of the patch, with a third slot positioned along the width, achieving an operational frequency of 4.8 GHz. In Step IV, L-shaped slots are symmetrically placed along the length and width of the square patch. Through optimisation of parameters such as lengths (l1, l2) and width (w1) of these slots, the final design operates at frequencies of 4.8 to 4.850 GHz and 6.28 to 6.295 GHz, as shown in Fig.2. Including L-shaped slots effectively extends the dimensions of the patch, resulting in a decrease in the operational frequency. Fig. 3 demonstrates carefully adjusting the feed point's position, dimensions, and slot placements to ensure effective operation within the sub-7 GHz band. The surface current distribution over the slots is analysed at 4.8 GHz and 6.29 GHz in Fig. 4. The resonant modes of these slots are meticulously aligned and matched at the specified frequencies. The introduction of L-shaped slots induces surface currents on the patch, generating circularly polarized radiation in both horizontal and vertical directions. This configuration achieves an Axial Ratio (AR) of less than 3 dB at the specified operating frequencies. Detailed discussions on radiation performance and axial ratio results are provided in subsequent sections.

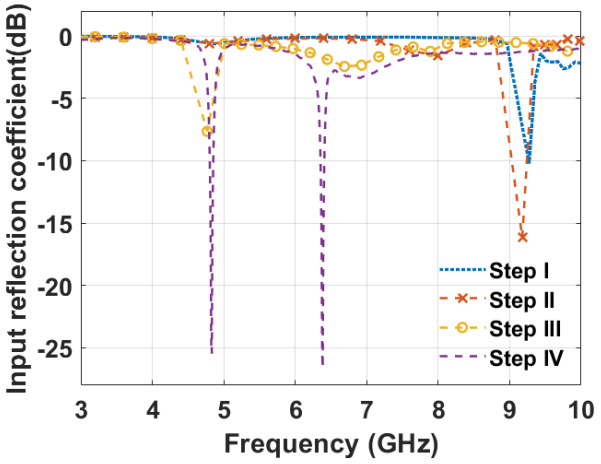

FIGURE 2. The S_{11} (dB) value of sub-7 GHz band antenna from step I to step IV as shown in Fig.1.

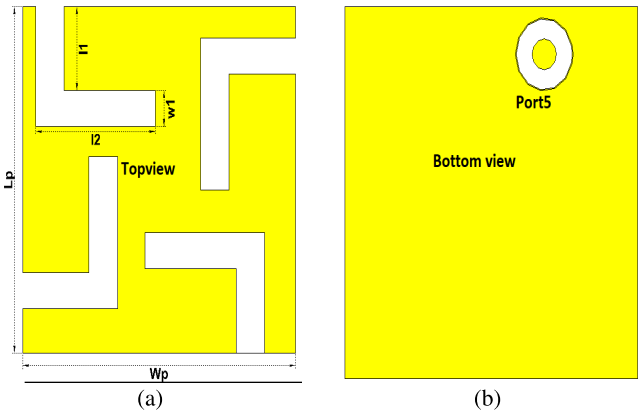

FIGURE 3. (a) Top view of a patch antenna with inverted L-shape slots design at sub-7 GHz band, (b) bottom view.

B. A DESIGN OF ANTENNA FOR KA-BAND

The design methodology of SIW structure, via dimensions and spacing, is followed as mentioned in [22]. The cutoff frequency operation of SIW, W_{eff}, and W_{siw} are calculated with the equations mentioned in [22]. The L_{siw} value is chosen $^{3\lambda}/_{2}$ at operating frequency 28 GHz. A grounded coplanar waveguide (GCPW) feed structure with width w_f and tapered slots width a is designed for the transition of TEM mode to TE_{10} mode. This transition structure allows the propagation of TE_{10} and higher order modes in SIW [23]. To excite the propagating modes in SIW, two resonating FKS slots with length l_s and width w_s are placed at $^{\lambda_g}/_{4}$ distance from the short end side of SIW as shown in Fig. 5. Two FKS slots are arranged at a distance of $^{\lambda_g}/_{2}$ in array model with 180^o phase shift, and placed at d_{offset} distance from the center acheive the overall shunt conductance g_n value is zero for

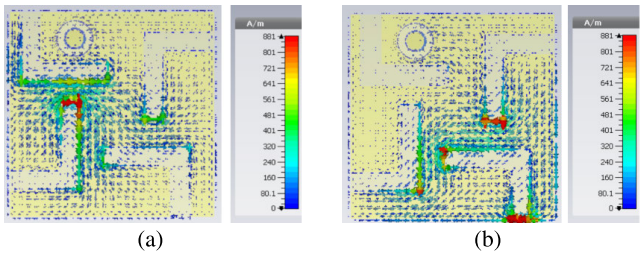

FIGURE 4. Surface current distribution on sub-7 GHz patch antenna at (a) a frequency of 4.8 GHz (b) a frequency of 6.29 GHz.

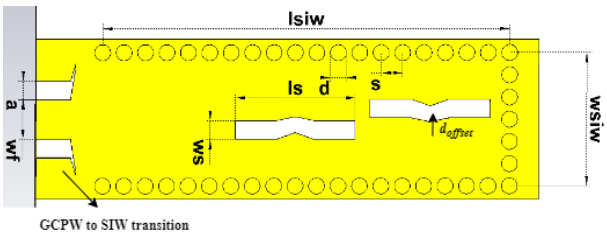

FIGURE 5. SIW FKS slotted array antenna at Ka-band.

TABLE 1. Optimized data for proposed ASA antenna.

Variable	dimensions (mm)	Variable	dimensions (mm)
W_{siw}	5	d	0.6
L_{siw}	15	s	1
l_s	4.53	w_s	0.7
K_t	0.25	d_{offset}	0.4
wf	1.0	a	0.7
Lp	12	Wp	12
$l2$	5	$l1$	4
$w1$	0.8	λ_g	9.06

impedance matching. By optimizing the fractal Koch depth K_t, and d_{offset} values, all the dimensions are mentioned in Table. 1, and resultant structure in Fig. 5, operating from 27.1 to 32.5 GHz.

III. RESULTS AND DISCUSSION

The S_{11} response for the proposed aperture-sharing antenna (ASA) is evaluated using the MS46122B Vector Network Analyzer (VNA), as shown in Fig. 6(b). During the S_{11} measurement within the sub-7 GHz band, the ka-band antenna elements are terminated with 50 Ω load. Likewise, the S11 of the Ka-band antenna is also measured. Fig. 7 compares the measured and simulation outcomes. The antenna for the sub-7 GHz band functions at a frequency of 4.8 GHz and 6.29 GHz, while the SIW slotted antenna operates in the range of 27.1 to 32.5 GHz, exhibiting a 20.3% bandwidth. In addition to analysing the input reflection coefficient, mutual coupling performance evaluation is essential to prevent grating lobes in radiation. The mutual coupling between antenna elements is decreased by the arrangement of Ka-band antenna elements in orthogonal directions, and this value is measured, as depicted in Fig. 8. The isolation between port five and the remaining ports is more than 60 dB at 4.8 GHz

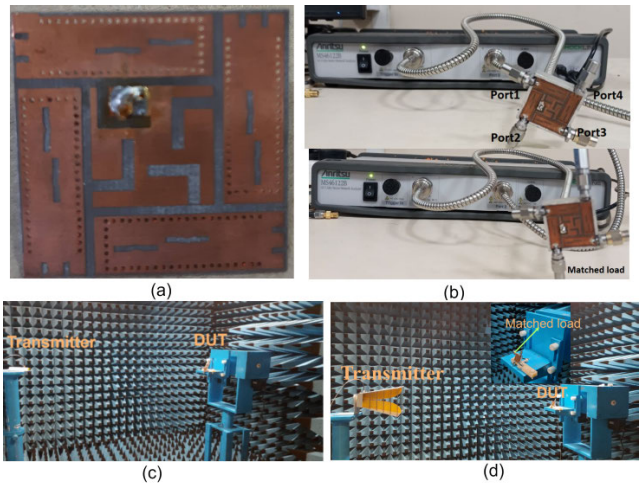

FIGURE 6. The measurement steps: (a) prototype (b) reflection coefficient and isolation parameters measurements using VNA MS46122B (c) Ka-band radiation performance measurement in an anechoic chamber. (d) sub-7 GHz band radiation performance measurement in an anechoic chamber.

and 6.29 GHz, achieved by SIW structure high-pass filter characteristics. The SIW structure exhibits high-pass filter attributes beyond the cutoff frequency, effectively attenuating sub-6 GHz band signals within the waveguide. This capability achieves substantial isolation between antennas, even during sub-6 GHz band operation. Moreover, Ka-band antennas are arranged orthogonally to achieve a 20 dB isolation at Ka-band operation, as depicted in Fig. 8 The radiation performance of the antenna is assessed within an anechoic chamber, as depicted in Fig. 6(c) and (d). Low-frequency band and Ka-band horn antennas are employed as transmitters to measure the radiation pattern, gain, and axial ratio (AR) at the sub-7 GHz and Ka bands, respectively. The radiation characteristics of the sub-7 GHz band antenna are measured in the YZ plane at the operating frequencies, and the corresponding results are presented in Fig. 9. The obtained values for gain and axial ratio (AR) of the sub-7 GHz band antenna, acquired through measurements and simulations, are illustrated in Fig. 10. At 4.8 GHz, the simulated and measured gain values for the low-frequency band antenna are 4.4 dBi and 4 dBi, respectively, while the AR values are 1.8 dB and 1.7 dB. The gain values at 6.29 GHz are 3.8 dBi and 3.76 dBi, respectively, whereas the AR values are 1.5 dB and 1.6 dB. The co-pol and cross-pol radiation patterns of the individual Ka-band antennas in the XZ and YZ planes are presented in Fig. 11. These antennas radiate broadside radiation with simulated and measured peak gains of 8.2 dBi and 8.4 dBi, respectively, and an AR of 40 dB over the operating band, as shown in Fig. 12.

A. MIMO PERFORMANCE

The investigation is centred on the evaluation of Ka-band antennas deployed in a MIMO configuration on a square-shaped substrate, as illustrated in Fig.1. The antennas'

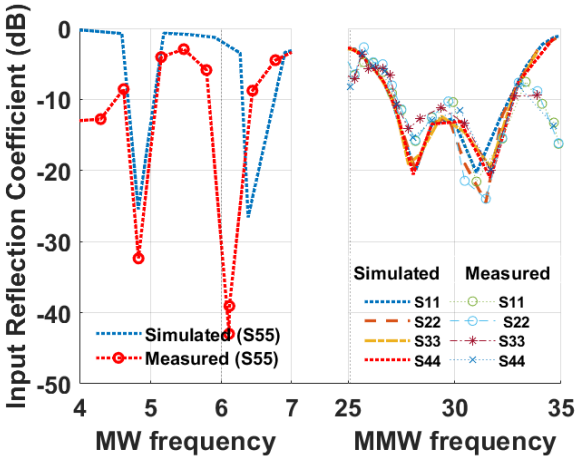

FIGURE 7. The aperture-shared antenna reflection co-efficient values at dual-band frequencies.

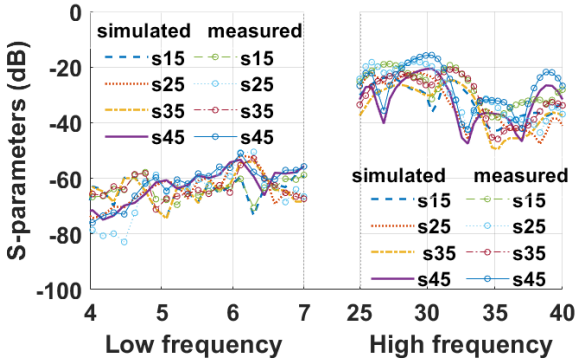

FIGURE 8. The mutual coupling performance of proposed dual-band antenna.

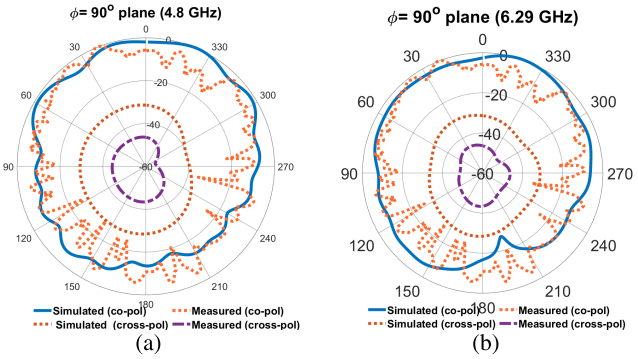

FIGURE 9. 2-D radiation pattern of sub-7 GHz band antenna (a) at 4.8 GHz (b) at 6.29 GHz.

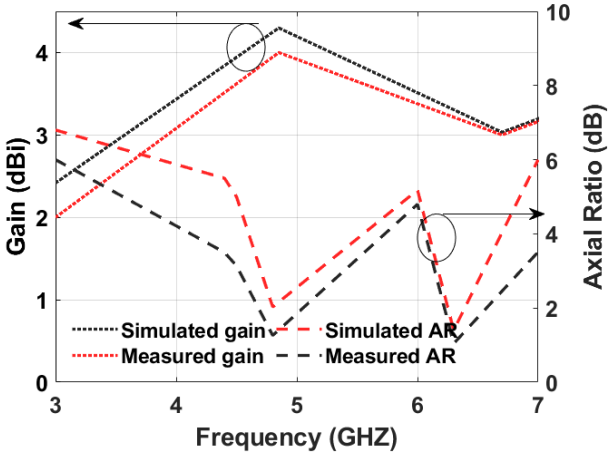

FIGURE 10. Axial ratio response over the operating frequency band of sub-7 GHz band antenna.

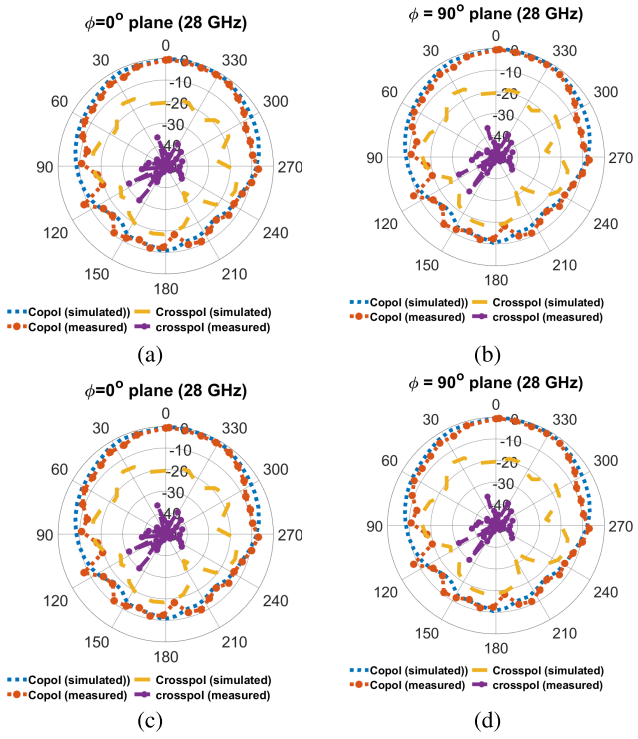

FIGURE 11. The four Ka-band antenna elements far-field patterns (a) XZ plane: radiator-1, (b) YZ plane: radiator-2, (c) XZ plane: radiator-3, and (d) YZ plane: radiator-4.

performance focuses explicitly on diversity characteristics. The Envelope Correlation Coefficient (ECC) is determined to be less than 0.01, indicating exceptional diversity performance. A measured Diversity Gain (DG) of 9.99 dB showcases the antenna's efficacy in achieving diversity. A Channel Capacity Loss (CCL) value of 0.1 bits/sec/Hz is also established, highlighting the antenna's suitability for 5G communication in MIMO systems. This study emphasizes the potential for high-capacity and dependable communication inherent in the performance of MIMO systems, as appraised through the outlined diversity characteristics in subsequent sections.

1. Envelope Correlation Coefficient (ECC)

ECC is a metric for diversity characteristics, calculated by assessing envelope correlation between individual antenna elements in a MIMO setup under isotropic conditions. The calculation involves using any two antenna far-field

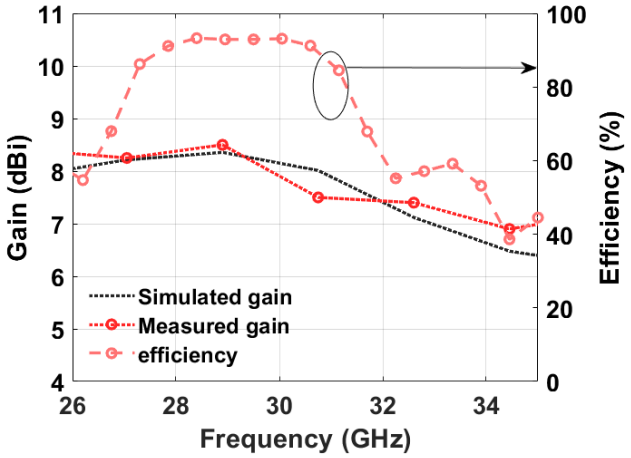

FIGURE 12. The gain performance of dual-band proposed antenna at ka-band.

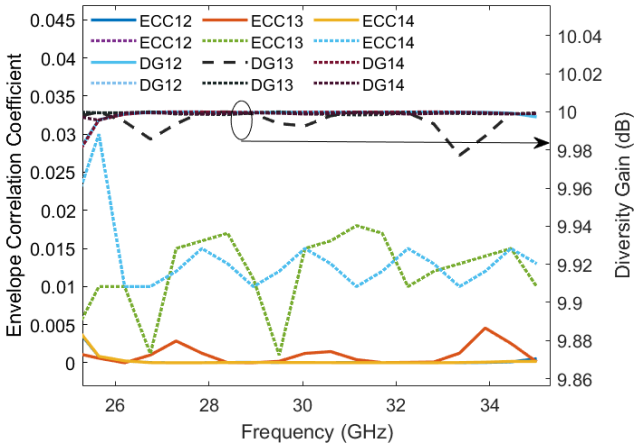

FIGURE 13. ECC and DG performance of MIMO antenna, '_____' is simulated '. . . .' is the measured value.

components as described. below Eq. 5 [24]

$$ECC_{mn} = \frac{\left| \int_0^{4\pi} \int \left[\overline{p}_m(\theta,\phi) \times \overline{p}_n(\theta,\phi)\right] d\Omega \right|^2}{\int_0^{4\pi} \int |\overline{p_m}(\theta,\phi)|^2 d\Omega \int_0^{4\pi} \int |\overline{p_n}(\theta,\phi)|^2 d\Omega} \tag{5}$$

$$ECC_{mn} = \frac{|s_{11}^* s_{12} + s_{21}^* s_{22}|^2}{(1-|s_{11}|^2-|s_{21}|^2) \times (1-|s_{22}|^2-|s_{12}|^2)} \tag{6}$$

where $\overline{p}_m(\theta,\phi)$,$\overline{p}_n(\theta,\phi)$ are the three-dimensional field patterns up on the excitation of m^{th} and n^{th} antenna, respectively, over the sphere, $d\Omega$ is the beam solid angle over the sphere. Ideally, uncorrelated antennas have zero ECC value. The simulated ECC value of the proposed MIMO antenna is less than 0.0005 in the operating band, while the measured ECC is calculated using the following Eq. 6. where s_{11}^* is the complex conjugative value of s_{11}, s_{12},s_{21} is mutual coupling between two antennas, s_{21}^* is a conjugated complex value, after taking measured values from VNA, the calculated ECC value is 0.01 which is far below the practical value (0.5). The ECC value within acceptable limits ensures that this design is suitable for functional MIMO systems, as shown in Fig.13.

B. DIVERSITY GAIN (DG)

The second aspect of diversity performance is Diversity Gain (DG), which signifies improved signal quality, particularly an increased signal-to-noise ratio (SNR) through the utilization of multiple antenna elements in communication, as opposed to a single element. It can be determined using Eq. 7 [25] by observing Fig. 13. The simulated and measured values are around 9.99 and 9.95 dB across the operating bandwidth, meeting the practical threshold of 10 dB.

$$DG = 10\sqrt{1-|0.99ECC|^2} \tag{7}$$

C. CHANNEL CAPACITY LOSS (CCL)

In MIMO systems, data handling capacity is crucial. More antennas at the transmitting end boost capacity and signal-to-noise ratio. However, increased elements also bring mutual coupling interference, leading to a reduction in data transmission capacity. This transmission loss at the Tx side of the channel is calculated with the following Eq. 8 [26].

$$CCL = -\log_2 \det(\Psi^R) \tag{8}$$

Ψ^R represents the correlation matrix with respective correlation coefficient values between antenna elements. The matrix and corresponding elements evaluation equation is represented in Eqs. (9), (10), and (11).

$$\psi^R = \begin{bmatrix} \rho_{11} & \rho_{12} \\ \rho_{21} & \rho_{22} \end{bmatrix} \tag{9}$$

$$\rho_{ii} = 1 - \sum_{n=1}^{2} (s_{in} * s_{ni}) \tag{10}$$

$$\rho_{ij} = -\sum_{n=1}^{2} (s_{in} * s_{nj}) \; For \; i,j = 1,2. \tag{11}$$

where ρ_{ii} is the correlation factor of identical antenna element, and ρ_{ij} are the correlation factor among the i^{th} and j^{th} nuber of antenna elements in the proposed design. Fig. 14 illustrates the proposed design, with modelled CCL at 0.1 bit/sec/Hz and measured CCL at 0.2 bit/sec/Hz, both falling within the acceptable limit of 0.6 bit/sec/Hz across the operational bandwidth. The performance of the proposed work is compared with prior research in Table 2 across various parameters such as frequency bands, size, number of layers, bandwidth, gain, channel isolation, and polarization. Notably, the proposed design achieves triple-frequency operation (4.8/6.2/28 GHz) with two operating frequencies in both the sub-7 GHz band and Ka-band, distinguishing it from previous works [14], [17], [20], and [27]. Those prior works are reported to have a sub-6 GHz band and

TABLE 2. Comparison of work with previously reported works.

Ref	Frequency (fl/fh) (GHz)	size (λ_1^3)	Layers	BW % (fh)	Gain (dBi)	isolation (dB)	Polarization
[14]	3.5/28	0.26*0.26*0.04	2	3.29	5.35/14.5	-	$LP, \pm 45^0$
[17]	3.5/28	0.50*0.40*0.0116	1	20.5	7/11	-	LP,LP
[20]	5.8/30	0.65*0.65*0.019	2	8.1	10.4/8.5	-	CP, LP
[27]	3.5/60	1.0*1.0*0.031	3	6.4	7.3/24	65/135	LP,LP
This work	4.8& 6.29/28	0.41*0.41*0.008	1	20.3	4.35/3.8/8.5	55/21	CP,CP,LP

λ_1 is based on lower cutoff frequency, BW: Bandwidth, CP: Circular Polarization, LP: Linear Polarization .

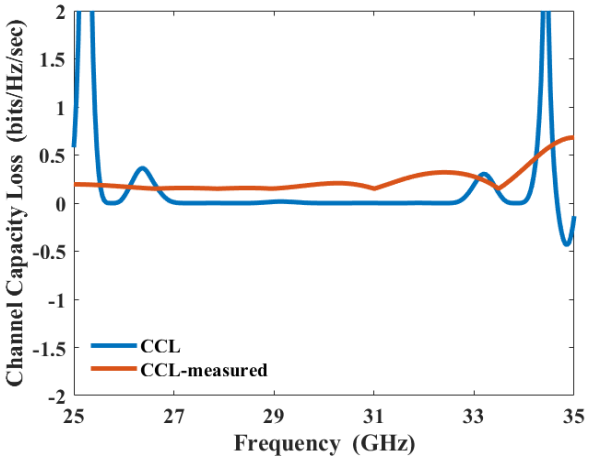

FIGURE 14. CCL values over the transmission in the operating frequency band.

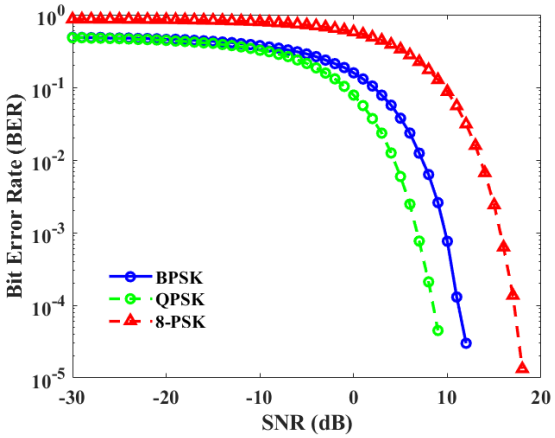

FIGURE 15. BER performance of MIMO antenna in AWGN channel.

Ka-band or V-band. This configuration offers the advantage of circular polarization during sub-7 GHz band operation, distinguishing it from [14], [17], and [27], where linear polarization is reported in low-frequency operation. The achieved wide bandwidth of 20.3% in the Ka-band facilitates faster communication, surpassing the bandwidths reported in [14] (3.29%), [20] (8.1%), and [27] (6.4%). In [17], yagi-uda elements utilizing SIW technology are reported with a bandwidth of 20.5% but with a high thickness profile, indicating that increased substrate thickness contributes to increased bandwidth. Furthermore, this structure attains a peak gain of 8.4 dBi with a single element, surpassing the peak gains reported in earlier studies such as [14], [17], and [27]. They employ three different architectures to enhance the gain: a 16-element cavity-backed slot array, a 4-element tapered slotted antenna array, and an array of 12 × 12 radiating elements in the SIW structure. Although the mentioned works lack information regarding channel isolation, [27] utilised a low pass filter based on a compact microstrip resonant cell (CMRC) structure for isolation enhancement. In contrast, the present work achieves satisfactory channel isolation without employing additional isolation elements, relying on the arrangement of elements in orthogonal directions. This comparative analysis suggests that this low-profile dual-polarized aperture shared antenna design with dual-band performance is well-suited for base station terminals in 5G and beyond wireless communications.

IV. MIMO ANTENNAS IN COMUNICATION

The proposed mm-wave wideband antenna can be operated as a transmitter (Tx) or receiver (Rx) antenna in massive MIMO systems. This MIMO antenna has four ports, which are orthogonally arranged to receive the vertical and horizontal radiation within the broadside direction. By accepting the orthogonally polarised signals, the interference can be reduced. At the receiver section, only one antenna receives maximum power from the transmitter of the same polarization and obtains good SNR. The proposed 2 × 2 MIMO antenna bit error rate (BER) performance is computed over the additive white Gaussian Noise (AWGN) channel. The antenna's carrier frequency is set to be 28 GHz, and 1×10^5 data bits are transmitted through the channel, and BER performance is evaluated for the MIMO antenna with three modulation technologies binary phase shift keying (BPSK), quadrature phase shift keying (QPSK), and 8-phase shift keying (8-PSK). Fig. 15 depicts that the BER value decreases exponentially as SNR increases. When the BER 1×10^{-4} SNR values of the MIMO antenna are between 10 to 15 dB for three modulation techniques. The proposed compact wideband antenna is a good choice for 5G applications, especially with micro base stations. It covers the bands of sub-7 GHz and FR2 (26-40 GHz).

V. CONCLUSION

An integrated single-layer dual-polarized antenna operating in both the sub-6GHz band (MW band), and the millimeter-wave (MMW) band (Ka: 26 – 40 GHz) is designed and

analysed. The Ka-band antenna is designed with a fractal Koch slot (FKS) to operate from 27.1 to 33.2 GHz with a 20.3 % bandwidth, suited for n257 band operation. A co-axial fed microstrip patch antenna was designed to achieve low-frequency operation at 4.8 and 6.29 GHz used for n77 (4400-5000 MHz) and n96 (5925-7125 MHz) bands of operation. The sub-7 Ghz band antenna exhibits circular polarisation, achieving a gain of 4.35 dBi and 3.8 dBi at 4.8 GHz and 6.29 GHz, respectively. The Ka-band antenna exhibits linear polarization and increases 8.5 dBi at 28 GHz. This Ka-band antenna Multiple Input Multiple Output (MIMO) characteristics are analysed, and the Envelope correlation coefficient (ECC) is 0.01, a Divesy gain of 9.98 dB, and Channel Capacity Loss (CCL) value of 0.1 bits/sec/Hz. The bit error rate performance of the MIMO antenna is analysed and achieves satisfactory value over binary phase shift keying (BPSK), quadrature phase shift keying (QPSK), and 8-phase shift keying (8-PSK). The integration of both Ka-band and sub-7 GHz band antennas in a single layer, possessing these characteristics, renders it suitable for deployment in base station terminals for 5G and upcoming wireless communication systems.

REFERENCES

[1] W. Hong, Z. H. Jiang, C. Yu, D. Hou, H. Wang, C. Guo, Y. Hu, L. Kuai, Y. Yu, Z. Jiang, Z. Chen, J. Chen, Z. Yu, J. Zhai, N. Zhang, L. Tian, F. Wu, G. Yang, Z.-C. Hao, and J. Y. Zhou, "The role of millimeter-wave technologies in 5G/6G wireless communications," *IEEE J. Microw.*, vol. 1, no. 1, pp. 101–122, Jan. 2021.

[2] Y. Zhu, G. Zheng, L. Wang, K.-K. Wong, and L. Zhao, "Content placement in cache-enabled sub-6 GHz and millimeter-wave multi-antenna dense small cell networks," *IEEE Trans. Wireless Commun.*, vol. 17, no. 5, pp. 2843–2856, May 2018.

[3] A. Pfadler, C. Ballesteros, J. Romeu, and L. Jofre, "Hybrid massive MIMO for urban V2I: Sub-6 GHz vs mmWave performance assessment," *IEEE Trans. Veh. Technol.*, vol. 69, no. 5, pp. 4652–4662, May 2020.

[4] M. Ko, H. Lee, and J. Choi, "Planar LTE/sub-6 GHz 5G MIMO antenna integrated with mmWave 5G beamforming phased array antennas for V2X applications," *IET Microw., Antennas Propag.*, vol. 14, no. 11, pp. 1283–1295, Sep. 2020.

[5] M. M. Sohul, M. Yao, T. Yang, and J. H. Reed, "Spectrum access system for the citizen broadband radio service," *IEEE Commun. Mag.*, vol. 53, no. 7, pp. 18–25, Jul. 2015.

[6] J. Gozalvez, "5G worldwide developments [mobile radio]," *IEEE Veh. Technol. Mag.*, vol. 12, no. 1, pp. 4–11, Mar. 2017.

[7] K. Shafique, B. A. Khawaja, F. Sabir, S. Qazi, and M. Mustaqim, "Internet of Things (IoT) for next-generation smart systems: A review of current challenges, future trends and prospects for emerging 5G-IoT scenarios," *IEEE Access*, vol. 8, pp. 23022–23040, 2020.

[8] H.-C. Huang and J. Lu, "Retrospect and prospect on integrations of millimeter-wave antennas and non-millimeter-wave antennas to mobile phones," *IEEE Access*, vol. 10, pp. 48904–48912, 2022.

[9] L. Chettri and R. Bera, "A comprehensive survey on Internet of Things (IoT) toward 5G wireless systems," *IEEE Internet Things J.*, vol. 7, no. 1, pp. 16–32, Jan. 2020.

[10] R. M. Moreno, J. Ala-Laurinaho, A. Khripkov, J. Ilvonen, and V. Viikari, "Dual-polarized mm-wave endfire antenna for mobile devices," *IEEE Trans. Antennas Propag.*, vol. 68, no. 8, pp. 5924–5934, Aug. 2020.

[11] Y.-W. Hsu, T.-C. Huang, H.-S. Lin, and Y.-C. Lin, "Dual-polarized quasi Yagi–Uda antennas with endfire radiation for millimeter-wave MIMO terminals," *IEEE Trans. Antennas Propag.*, vol. 65, no. 12, pp. 6282–6289, Dec. 2017.

[12] M. Ikram, E. A. Abbas, N. Nguyen-Trong, K. H. Sayidmarie, and A. Abbosh, "Integrated frequency-reconfigurable slot antenna and connected slot antenna array for 4G and 5G mobile handsets," *IEEE Trans. Antennas Propag.*, vol. 67, no. 12, pp. 7225–7233, Dec. 2019.

[13] Y. Liu, Y. Li, L. Ge, J. Wang, and B. Ai, "A compact hepta-band mode-composite antenna for sub (6, 28, and 38) GHz applications," *IEEE Trans. Antennas Propag.*, vol. 68, no. 4, pp. 2593–2602, Apr. 2020.

[14] J. H. Bae and Y. J. Yoon, "5G dual (S-/Ka-) band antenna using thick patch containing slotted cavity array," *IEEE Antennas Wireless Propag. Lett.*, vol. 20, pp. 1008–1012, 2021.

[15] D. Wang and C. H. Chan, "Multiband antenna for WiFi and WiGig communications," *IEEE Antennas Wireless Propag. Lett.*, vol. 15, pp. 309–312, 2016.

[16] M. Ikram, N. Nguyen-Trong, and A. M. Abbosh, "Realization of a tapered slot array as both decoupling and radiating structure for 4G/5G wireless devices," *IEEE Access*, vol. 7, pp. 159112–159118, 2019.

[17] J. Lan, Z. Yu, J. Zhou, and W. Hong, "An aperture-sharing array for (3.5, 28) GHz terminals with steerable beam in millimeter-wave band," *IEEE Trans. Antennas Propag.*, vol. 68, no. 5, pp. 4114–4119, May 2020.

[18] R. Emrick, P. Cruz, N. B. Carvalho, S. Gao, R. Quay, and P. Waltereit, "The sky's the limit: Key technology and market trends in satellite communications," *IEEE Microw. Mag.*, vol. 15, no. 2, pp. 65–78, Mar. 2014.

[19] S. Ji, Y. Dong, S. Wen, and Y. Fan, "C/X dual-band circularly polarized shared-aperture antenna," *IEEE Antennas Wireless Propag. Lett.*, vol. 20, pp. 2334–2338, 2021.

[20] B. J. Xiang, S. Y. Zheng, H. Wong, Y. M. Pan, K. X. Wang, and M. H. Xia, "A flexible dual-band antenna with large frequency ratio and different radiation properties over the two bands," *IEEE Trans. Antennas Propag.*, vol. 66, no. 2, pp. 657–667, Feb. 2018.

[21] C. A. Balanis, *Antenna Theory: Analysis and Design*. Hoboken, NJ, USA: Wiley, 2016.

[22] E. Aparna, G. Ram, and G. A. Kumar, "Review on substrate integrated waveguide cavity backed slot antennas," *IEEE Access*, vol. 10, pp. 133504–133525, 2022.

[23] S. G. Mallick, G. A. Kumar, S. Chatterjee, B. Biswas, and D. R. Poddar, "Transitions from SIW to various transmission lines for substrate integrated circuits," in *Proc. URSI Asia–Pacific Radio Sci. Conf. (AP-RASC)*, Mar. 2019, pp. 1–4.

[24] U. Sharma, G. Srivastava, and M. K. Khandelwal, "Quad-band two-port MIMO antenna serving for sub-7 GHz frequency with integrated circularly polarized bands," *AEU Int. J. Electron. Commun.*, vol. 160, Feb. 2023, Art. no. 154503.

[25] A. Iqbal, O. A. Saraereh, A. W. Ahmad, and S. Bashir, "Mutual coupling reduction using F-shaped stubs in UWB-MIMO antenna," *IEEE Access*, vol. 6, pp. 2755–2759, 2018.

[26] M. Khalid, S. I. Naqvi, N. Hussain, M. Rahman, Fawad, S. S. Mirjavadi, M. J. Khan, and Y. Amin, "4-port MIMO antenna with defected ground structure for 5G millimeter wave applications," *Electronics*, vol. 9, no. 1, p. 71, Jan. 2020.

[27] J. F. Zhang, Y. J. Cheng, Y. R. Ding, and C. X. Bai, "A dual-band shared-aperture antenna with large frequency ratio, high aperture reuse efficiency, and high channel isolation," *IEEE Trans. Antennas Propag.*, vol. 67, no. 2, pp. 853–860, Feb. 2019.

ELAGANDULA APARNA (Graduate Student Member, IEEE) received the B.Tech. degree in electronics and communication engineering from the Jawaharlal Nehru Technological University Hyderabad College of Engineering Jagtial and the M.E. (M.R.E.) degree from the University College of Engineering, Osmania University, Hyderabad, in 2015. She is currently a full-time Research Scholar with the Department of ECE, National Institute of Technology at Warangal, Warangal, India, with an Institute Fellowship from the Ministry of Human Resource Department (MHRD). Her research interests include antenna designs for 5G and beyond applications.

GOPI RAM (Senior Member, IEEE) received the B.E. degree in electronics and telecommunication engineering from the Government Engineering College, Jagdalpur, Chhattisgarh, India, in 2007, and the M.Tech. degree in telecommunication engineering from the National Institute of Technology Durgapur, Durgapur, West Bengal, India, in 2011. In 2012, he joined as a full-time Institute Research Scholar with the National Institute of Technology Durgapur, to carry out research the Ph.D. degree. He received the Scholarship from the Ministry of Human Resource and Development (MHRD), Government of India, from 2009 to 2011 (M.Tech. degree) and from 2012 to 2016 (Ph.D. degree). He has published more than 80 research papers in international journals and conferences. His research interests include the analysis and synthesis of antenna arrays via bio-inspired evolutionary algorithms and antenna array optimization of various radiation characteristics.

G. ARUN KUMAR (Senior Member, IEEE) was born in Hyderabad, India, in 1982. He received the B.E. degree in electronics and communications engineering from Osmania University, in 2004, and the M.E.Tel.E. and Ph.D. degrees in electronics and telecommunications engineering from Jadavpur University, in 2006 and 2012, respectively. He joined the Circuits and Systems Division, Society for Applied Microwave Electronic Engineering and Research (SAMEER), Kolkata, India, under the Ministry of Electronics and Information Technology (MeitY), Government of India, in 2010, where he was a Scientist B, from 2010 to 2014, and a Scientist-C, from 2014 to 2018. In June 2018, he joined the Department of Electronics and Communication Engineering, National Institute of Technology at Warangal, Warangal, where he is currently an Assistant Professor. He has completed two projects sponsored by DRDO and more than ten projects sponsored by MeitY. His research interests include simulation, modeling, and design of millimeter wave active and passive circuits, MMIC design, metamaterials, time-modulated components, and substrate-integrated waveguide circuits. He is a Life Member of IETE and the Society of EMC Engineers, India. He received the Early Career Research Award from DST-SERB, in 2019.